

Green Chemistry

Accepted Manuscript



This is an *Accepted Manuscript*, which has been through the Royal Society of Chemistry peer review process and has been accepted for publication.

Accepted Manuscripts are published online shortly after acceptance, before technical editing, formatting and proof reading. Using this free service, authors can make their results available to the community, in citable form, before we publish the edited article. We will replace this *Accepted Manuscript* with the edited and formatted *Advance Article* as soon as it is available.

You can find more information about *Accepted Manuscripts* in the [Information for Authors](#).

Please note that technical editing may introduce minor changes to the text and/or graphics, which may alter content. The journal's standard [Terms & Conditions](#) and the [Ethical guidelines](#) still apply. In no event shall the Royal Society of Chemistry be held responsible for any errors or omissions in this *Accepted Manuscript* or any consequences arising from the use of any information it contains.



www.rsc.org/greenchem

ARTICLE

Inspired by Bread Leavening: One-pot Synthesis of Hierarchically Porous Carbon for Supercapacitors

Cite this: DOI: 10.1039/x0xx00000x

Jiang Deng,^a Tianyi Xiong,^a Fan Xu,^a Mingming Li,^a Chuanlong Han,^a Yutong Gong,^a Haiyan Wang^a and Yong Wang^{a*}

Received 00th January 2012,

Accepted 00th January 2012

DOI: 10.1039/x0xx00000x

www.rsc.org/

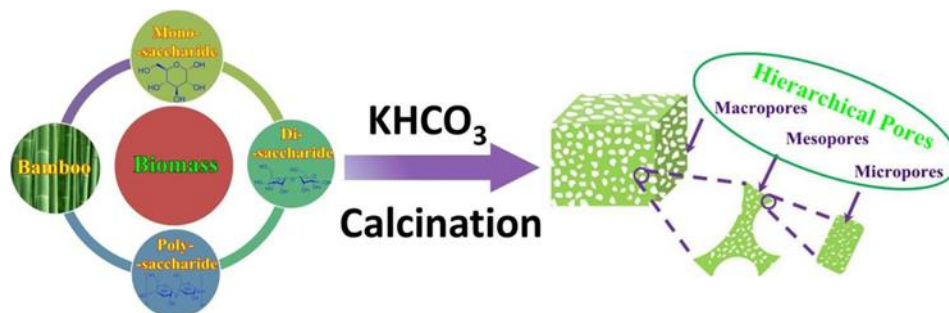
Hierarchically porous carbons (HPCs) show great potentials in energy storage due to their high surface area as well as short ion transport path derived from the interconnected porous framework. However, most existing protocols highly rely on the nanocasting and soft-templating, which usually restrict the using of raw materials and thus industrial unfeasible. It still reminds a big challenge to build HPCs from crude biomass, which is abundant on the earth, through a simply one-pot approach. Inspired by leavening bread, we design a strategy to fabricate HPCs with three-dimensional (3D) hierarchical pores consisting of macro, meso, and micropores. The "leavening method" is conducted simply by mixing the biomass with KHCO_3 followed by undergoing elevated temperature treatment. Besides the well-defined hierarchical structure, the as-prepared HPCs also exhibit notably large specific areas (up to $1893 \text{ m}^2 \text{ g}^{-1}$). It is noteworthy that this "leavening" strategy is widely applicable for most of biomass derivatives and biomass, including glucose, cellulose, chitin, starch, rice straw, bamboo, and etc. When evaluated as supercapacitor electrode materials in two-electrode test systems, the as-prepared HPCs exhibit an excellent electrochemical performance: specific capacitance of 253 F g^{-1} , almost no capacitance loss after 10 000 cycles.

Introduction

Due to the wide availability and superior physicochemical properties, porous carbon materials have been widely adopted as adsorbents,¹⁻³ catalyst supports^{4, 5} and carbon electrodes.⁶⁻⁹ Recently, porous carbon materials have been utilized in energy conversion and storage especially in supercapacitors due to their high specific surface area, excellent electrical conductivity and tunable pore size.¹⁰ For a long time, activated carbon, because of its high surface areas and pore volumes gained by selecting suitable precursors and activators, has been applied in supercapacitors.^{11, 12} However, activated carbon was only restricted to inferior ability in supercapacitor performance, as the pores are mainly restricted to micropores, which are not favorable for efficient electrolyte ion diffusion.¹³ Thus, besides the basic requirement of high surface area and large pore volume, suitable pore structure matters more for a good supercapacitor performance.¹⁴ Notably, the importance of pore types (Namely, micro-, meso- and macropores) in the supercapacitor performance is as follows: the presence of micropores accessible to the electrolyte ions are essential for high energy storage, meanwhile, mesopores can accelerate the kinetic process of the ion diffusion in the electrodes and

improve the power performance at high current densities; macropores serve as ion-buffering reservoirs, which can provide a short diffusion distance and facilitate the rapid transport of electrolyte ions.^{15, 16} Thus, it shows great potentials in supercapacitors with high performance to develop 3D HPCs (containing micro-, meso- and macropores).

Recently, the pursuit of high surface area with tunable hierarchical pores has therefore stimulated continuous efforts in developing more efficient synthetic routes for porous carbons.^{17, 18} Among the various synthetic methods, the nanocasting and soft-templating methods are widely used for the preparation of porous carbon.¹⁹⁻²³ Nevertheless, both nanocasting and soft-templating methods are very fussy, high-cost, and thus industrial unfeasible. Considering environment and sustainability issues, the synthetic strategies should be green and sustainable. In this regard, the recently developed environmentally friendly hydrothermal carbonization (HTC) of biomass is greatly desirable due to the use of renewable carbon sources.²⁴ To introduce appropriate porous texture, an activated process using suitable activators such as KOH ²⁵⁻²⁸ and ZnCl_2 ²⁹ were always performed. However, apart from the drawback of corrosion and massive use of KOH and ZnCl_2 , the developed structure of carbon is almost totally composed of micropores,



Scheme 1 Scheme diagram of the formation of C_{x-LE} : mixing the biomass with the “leavening” agents, followed by calcination under the insert gas for the synthesis of C_{x-LE} .

which is not convenient for mass transfer and therefore limited their applications. Very recently, Liu and co-workers³⁰ synthesized porous carbon through a molten salt activation route by using glucose as the model carbon precursor in molten LiCl/KCl containing different dissolved oxysalts. The process provides an effective route to convert biomass molecules to functional carbon-based nanomaterials which show large specific surface areas ($\sim 2000 \text{ m}^2 \text{ g}^{-1}$). However, the process consume large amount of LiCl/KCl (the mass ratio of molten salt to glucose is 10:1) and long calcination time. Hence, there is still a need for the development of low-cost, sustainable and general synthesis techniques for 3D HPCs with highly accessible surface areas and tunable pore texture.

Our concept was inspired by the fact that bread making would use gas-producing reagents such as yeast and baking soda to obtain porous structure. Because of the expanding of gas produced during baking or leavening process, the bread would acquire porous structure. It motivates us to use gas-producing chemicals during the carbonization process of biomass. Thus, we designed an activator-assisted pyrolysis route to prepare the 3D HPCs (the products prepared through “leavening” method are dubbed as C_{x-LE} and the products prepared via pyrolysis without additives are labeled as C_x , where x stands for first three letters of the carbon precursors.) (Scheme 1). The as-prepared products exhibit high specific surface area (Table S1, up to $1893 \text{ m}^2 \text{ g}^{-1}$) and a well-developed 3D hierarchically porous texture consisting of macro, meso and micropores. The average size of the macropores and the specific surface area can be controlled by the variation of the thermal treatment temperature, the heating rate and the ratio of the activator/precursors. Moreover, this method can be successfully applied to most of the biomass derivatives (xylose, glucose, sucrose, cellulose, starch, and chitin) and the crude biomass (straw and bamboo). Electrochemical tests showed that these high surface area 3D HPCs materials exhibited excellent electrochemical performance as a supercapacitor electrode material.

Results and discussion

The porous structure of the C_{cel-LE} was characterized by scanning electron microscopy (SEM) and transmission electron

microscopy (TEM). SEM images (Fig. 1b) shows a 3D frameworks with randomly opened macropores ranging from a few hundred nanometers to several micrometers. The TEM image (Fig. 1c) are consistent with the macropores observed in the SEM images (Fig. 1b). The mesoporous texture of the walls can be disclosed from the enlarged TEM images (Fig. 1d and Fig. S1). Also, the ultrathin carbon nanosheets (highlight by arrow on the Fig. 1c and 1d) can be also seen from the C_{cel-LE} , which have been also reported by other works,³¹ resulting from the expanding gases. In contrast, the SEM image (Fig. 1a) of the C_{cel} show monolithic morphology without macropores. Also, the TEM image (Fig. S2) of C_{cel} , which show no macropores and mesopores, is in corresponding with the SEM image.

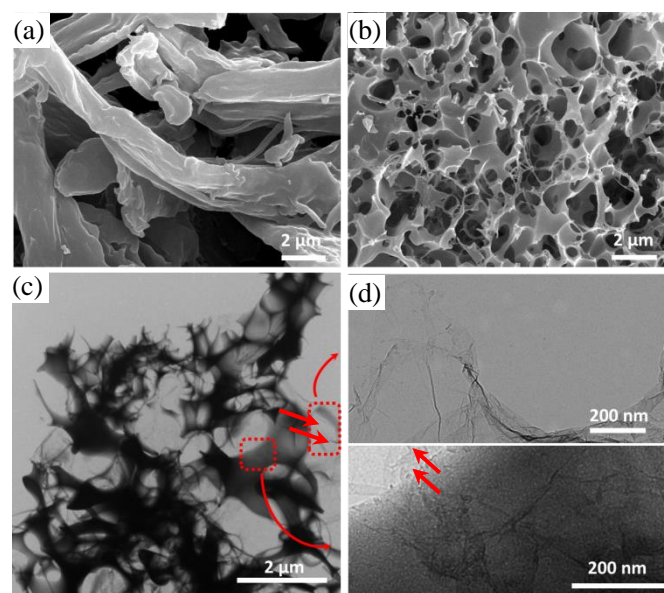


Fig. 1 SEM images of (a) C_{cel-LE} , (b) C_{cel} ; TEM images of (c) C_{cel-LE} , (d) enlarged TEM images of C_{cel-LE} (cel represents the cellulose).

The porosity of C_{cel-LE} and C_{cel} was then characterized by nitrogen sorption isothermal analysis. C_{cel} (Fig. 2a) exhibits a typical type I adsorption–desorption isotherm, indicating a microporous structure only. Whereas, C_{cel-LE} (Fig. 2a) is steep at low pressure in which micropore filling occurs, as well as the linear plot of nitrogen isotherms that reveal pore condensation

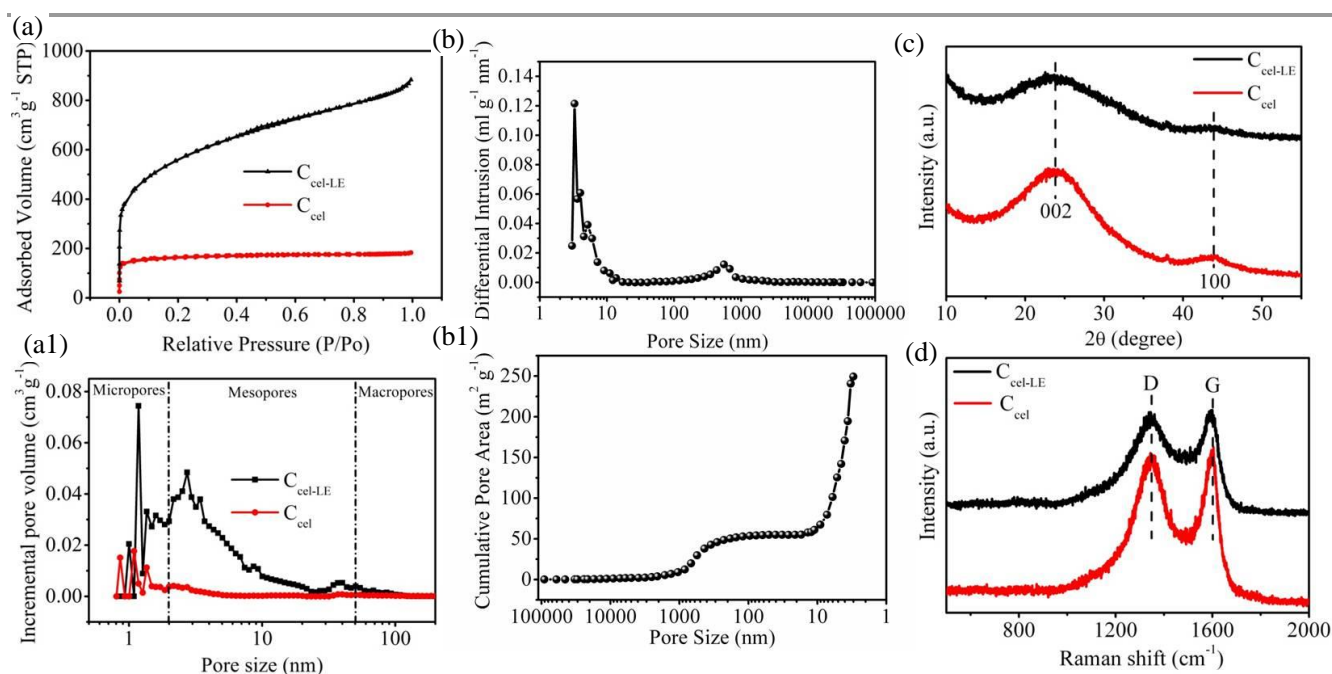


Fig. 2. (a) N_2 isotherms of the $C_{\text{cel-LE}}$ and C_{cel} and (a1) PSDs of $C_{\text{cel-LE}}$ and C_{cel} using the DFT model; (b) cumulative pore area of the $C_{\text{cel-LE}}$ measured by mercury porosimetry (b1) Macro-pore volume distributions for $C_{\text{cel-LE}}$ measured by mercury porosimetry; (c) XRD results of $C_{\text{cel-LE}}$ and C_{cel} ; (d) Raman spectra using 514 nm excitation of $C_{\text{cel-LE}}$ and C_{cel} .

and type H2 hysteresis, which is indicative of an interconnected pore system exhibiting constrictions. From these isotherms, it turned out that $C_{\text{cel-LE}}$ holds remarkably higher specific surface area and pore volume than those of C_{cel} when analyzing on the basis of the Brunauer–Emmett–Teller (BET) and Barrett–Joyner–Halenda (BJH) model, respectively: 1893 versus 506 $\text{m}^2 \text{g}^{-1}$ and 1.37 versus 0.46 $\text{cm}^3 \text{g}^{-1}$. Also, $V_{\text{mic}}/V_{\text{total}}$ (The volume ratio of micropores to total) of C_{cel} and $C_{\text{cel-LE}}$ are 0.68 and 0.18, respectively, which suggest the great increasing of mesopores volume when executing the “leavening” method. (Table S1). Fig. 2a1 displays the DFT pore size distribution (PSD) from nitrogen adsorption. Unlike C_{cel} , which indicates the microporous texture only, the $C_{\text{cel-LE}}$ has a well-defined micro-meso-macropore size distribution. Also, the macropore volume distributions and the porosity of $C_{\text{cel-LE}}$ were measured by Hg porosimetry. Fig. 2b displays the PSD obtained through hydrargyrum pressing method. Besides the mesopores peaked at 3.2 nm, $C_{\text{cel-LE}}$ has macropores peaked at 548 nm which is consistent with the results from the SEM images (Fig. 1b) and the cumulative pore area image (Fig. 2b1). Furthermore, the bulk density and the apparent density are as low as 0.043 g cm^{-3} and 0.296 g cm^{-3} , respectively. The bulk densities result in the porosity of 85.5%, which demonstrates rich macropores.³² On the basis of the above analysis, the sample prepared through our “leavening” strategy shows high specific surface area and large volume with hierarchical micro-meso-macro pores.

The samples were subjected to X-ray diffraction (XRD) analysis to characterize the local atomic structure. The XRD spectrum (Fig. S3) of $C_{\text{cel-LE}}$ before etched by HCl solution reveals the existence of K_2CO_3 (PDF#49-1093), which indicate

that KHCO_3 decomposed into K_2CO_3 at elevated temperature. There are not any peaks of K_2CO_3 in the XRD spectrum of $C_{\text{cel-LE}}$ (Fig. 2c), which exhibit K_2CO_3 have been removed thoroughly through the etching process. Moreover, $C_{\text{cel-LE}}$ and C_{cel} are both typical disordered glassy polymer without pronounced order, as suggested by the broadened humps in the XRD patterns (Fig. 2c). For the C_{cel} , the diffraction peak at a 2θ value of 44° can be assigned as the (100) reflection of graphite. Comparing with the intensity of (002) peaks, it is obvious that the graphitization degrees of $C_{\text{cel-LE}}$ are lower than that of C_{cel} .³³ The same conclusion can also be drawn from the Raman spectra (Fig. 2d), in which the G band at $\sim 1603 \text{ cm}^{-1}$ demonstrates the in-plane vibration of the sp^2 carbon atoms, while the D band at $\sim 1343 \text{ cm}^{-1}$ is a defect-induced Raman feature representing the non-perfect crystalline structure of the material. The $I_{\text{G}}/I_{\text{D}}$ (I_{D} represents the intensity of the D band, and I_{G} stands for the intensity of the G band) of $C_{\text{cel-LE}}$ is lower than that of C_{cel} , suggesting more defective structure with lower graphitization. It seems that the activator would corrode the graphitic structure, leading to a more defective texture.

The influence of temperature on the morphology and the pore structure was investigated. From the SEM images (Fig. S4), the macropores can be seen for all the products. When temperatures were increased from 400 $^\circ\text{C}$ to 800 $^\circ\text{C}$, the pore wall would become thinner. Because of the molten state of activator at 900 $^\circ\text{C}$, the carbon would self-shrink and lead to thicker pore wall. In addition, the specific surface areas and the average macroporous size rose as temperature increased (Fig. S5b), which can be ascribed to the interconnection of adjacent pores caused by the activator corrosion. While the $V_{\text{mic}}/V_{\text{total}}$ of

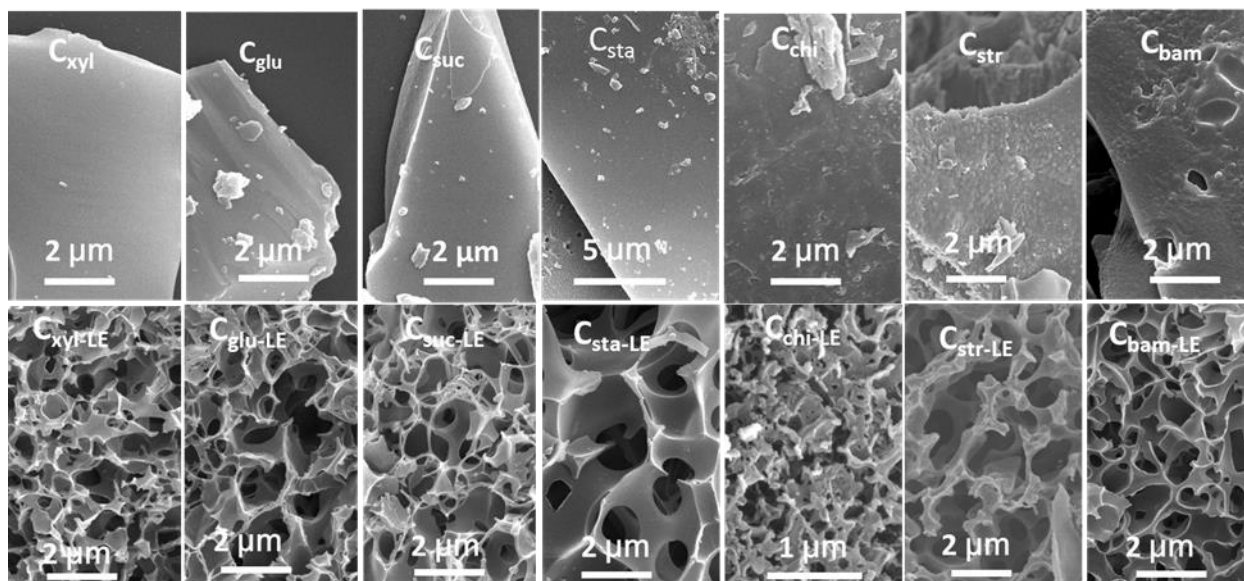


Fig. 3 SEM images of C_{x-LE} and C_x where x is the carbon precursors (xyl, glu, suc, sta, chi, str, and bam represent xylose, glucose, sucrose, starch, chitin, straw, and bamboo, respectively).

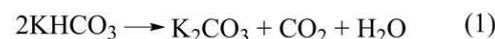
the as-prepared products greatly increased at first and decreased later (Table S2 and Fig. S5a), which would be discussed in detail later on. However, there was little product when the temperature increased to 1000 °C. It means that a proper calcination temperature ensure a high specific surface area with a appropriate yield. Meanwhile, the elementary analysis (EA) (Table S3 and S4) shows that the content of carbon also rise as the temperature increased, which demonstrate higher temperature leads to higher degree of graphitization. The X-ray diffraction patterns showed that all the products have similar graphitic structure (Fig. S6a). Furthermore, the Raman spectra of these carbon products with different heat treatments (Fig. S6b) clearly show relatively broad and weak D and G bands, which suggest the presence of significant amounts of disordered carbon.

The control of specific surface areas and the macropore size was also studied by adjusting the cellulose/ $KHCO_3$ ratio. When the weight ratio of the activator to cellulose varied from 2 to 8, the corresponding specific surface areas were first increased from 1690 to 1893 $m^2 g^{-1}$ and then decreased to $\sim 1709 m^2 g^{-1}$ (Table S1 and Fig. S5c). It seems that a suitable V_{mic}/V_{total} is indispensable to ensure the high specific surface area. Accordingly, when the weight ratio of activator to the cellulose is adjusted to 4, the content of carbon is the highest (Table S4). However, the average macroporous size decreased when the mass of activator increased, which may be ascribed to the shrinking of the carbon framework (Fig. S5d).

The “leavening” strategy was also implemented on other biomass and biomass derivatives. Fig. 3 showed whatever biomass derivatives (xylose, glucose, sucrose, starch, and chitin) or crude biomass (straw and bamboo), the similar morphology as the C_{cel-LE} can be seen for all the products synthesized through the “leavening” protocol. Further, Table S5 and Fig. S7

demonstrate similar high specific surface areas with hierarchically porous structure of the samples synthesized via the “leavening” method. However, the products without adding the activator all show bulk morphology. There is no doubt that the “leavening” strategy is universal and show great potential for industrialization application.

Thermogravimetric analysis (TGA) (Fig. S8) was performed on the cellulose and the mixture (the mass ratio of $KHCO_3$ to cellulose is 4:1) to give a further insight of the pyrolysis process. The initial weight loss for both samples below 200 °C was due to desorption of water. The cellulose lost the most weight between 300 and 400 °C, which is due to the carbonization of the cellulose. Whereas, for the mixture, the derivative thermogravimetric (DTG) curves show two weight loss peaks at ~ 220 °C and ~ 270 °C, respectively. Obviously, the mixture showed a ~ 25 wt % weight loss at the first weight loss peak, which is equal to weight loss calculated theoretically (the procedure is shown detailly in the Supporting Information). It presented that $KHCO_3$ decomposed via reaction (equation (1) list below). The K_2CO_3 formed via the decomposition of $KHCO_3$ would fuse at 900 °C (the fusion point of K_2CO_3 is



891 °C), where the porous carbon framework would shrink. The weight loss peak at ~ 270 °C for the mixture was ascribed to the decomposition of the cellulose, which is lower than

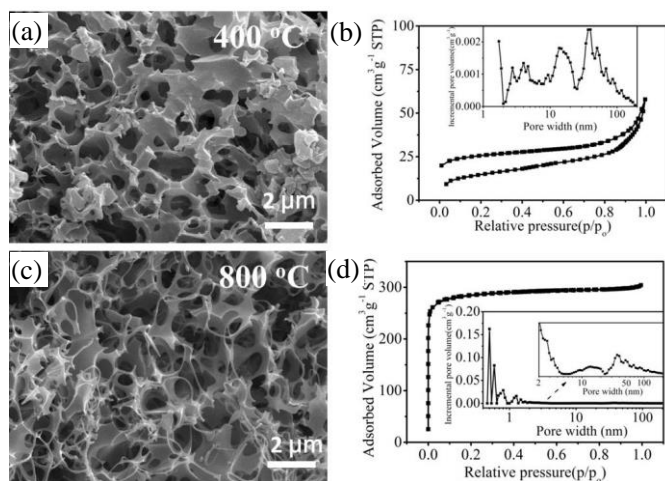


Fig. 4 SEM images of C_{cel-LE} prepared at (a) 400 °C (c) 800 °C; N₂ sorption isotherms of C_{cel-LE} prepared at (b) 400 °C (d) 800 °C.

decomposition temperature of the pure cellulose. With the above observations, the KHCO₃ activator may also function to catalyze the decomposition of cellulose because of the weak alkalinity of the activator.

Concerning the formation mechanism of the HPCs, it is in general accepted that mesopores and micropores are generated by the reaction between the activator and the as-formed carbon intermediate, which is similar to the traditional activating route.^{26,34} However, the formation mechanism of the macropores still remained to be uncovered. Based on our observations, the development of macropores during pyrolysis process resembles the leavening procedure of flour. That is, gas produced by the decomposition of KHCO₃ (equation (1) list above) dilated and produced the macropores. To verify our hypothesis, the calcination of mixture (the mass ratio of KHCO₃ to cellulose is 4:1) was conducted at 400 °C, under which only reaction (equation (1) list above) would take place at this temperature. As expected, the product exhibits macroporous structure (Fig. 4a) with little micropores and mesopores (Fig. 4b and Table S2). Moreover, the average macropore size increased when the heat rate enhanced (Fig. S9) because of the quicker decomposition rate of KHCO₃. To further verify the importance of the decomposition of KHCO₃, the calcination of mixture (where the KHCO₃ was replaced by K₂CO₃) was conducted at 400 °C too. However, the as-obtained products do not exhibit any more macroporosity (Fig. S10). When temperature is above 800 °C, reactions (equation (2-5) list above) would occur.²⁶ The nitrogen sorption isotherm and PSD (Fig. 4d) show that the sample possesses rich micropores and mesopores as well as the macropores (Fig. 4c). Besides, the pore wall becomes thinner due to the reactions between the carbons and the activator. So the average macropore size is larger when the temperature increased (Fig. S5b). Note that the mixture of cellulose and activators which are gas-producing chemicals would obey the same mechanism during calcination. When KHCO₃ was replaced by NaHCO₃, the as-prepared product also presents macroporosity (Fig. S11).

The as-prepared samples possess high specific surface area, well-defined hierarchical pores (containing micro-, meso- and macropores) and good electronic conductivity, which guarantee a good performance when measured as supercapacitors.^{35, 36} C_{cel-LE} and C_{bam-LE} were chosen as representative to explore their performance of supercapacitors.³⁷ Other control samples including C_{cel} and C_{bam} were also tested for comparison. The cyclic voltammograms (CV) curves between -1.0 and 0 V of electrode materials at 50 mV s⁻¹ reveal a typical capacitive behavior (Fig. 5a). Compared to the CV curves of C_{cel} and C_{bam}, CV curves of C_{cel-LE} and C_{bam-LE} show quasi-rectangular shape, demonstrating a typical characteristic of double-layer capacitance with little electrolyte diffusion limitation.³⁸ The tiny deformation of CV curves of C_{cel-LE} and C_{bam-LE} may be ascribed to the pseudocapacitance derived from oxygen-containing functional groups in the carbon materials. (Fig. S12 and S13) The galvanostatic charge/discharge curves obtained at 0.5 A g⁻¹ (Fig. 5b) reveal almost symmetrical triangle. C_{cel-LE} and C_{bam-LE} give a specific capacitance of 253 F g⁻¹ and 187 F g⁻¹, respectively, which are much higher than 93 F g⁻¹ of C_{cel} and 61 F g⁻¹ of C_{bam} at a low current density of 0.1 A g⁻¹ (Fig. S14). These excellent performance of such porous carbons prepared through “leavening” method are attributed to their 3D hierarchically porous structure in the continuous carbon framework. The macro&meso pores may serve as the buffering reservoirs, while the mesoµ pores may supply adsorption

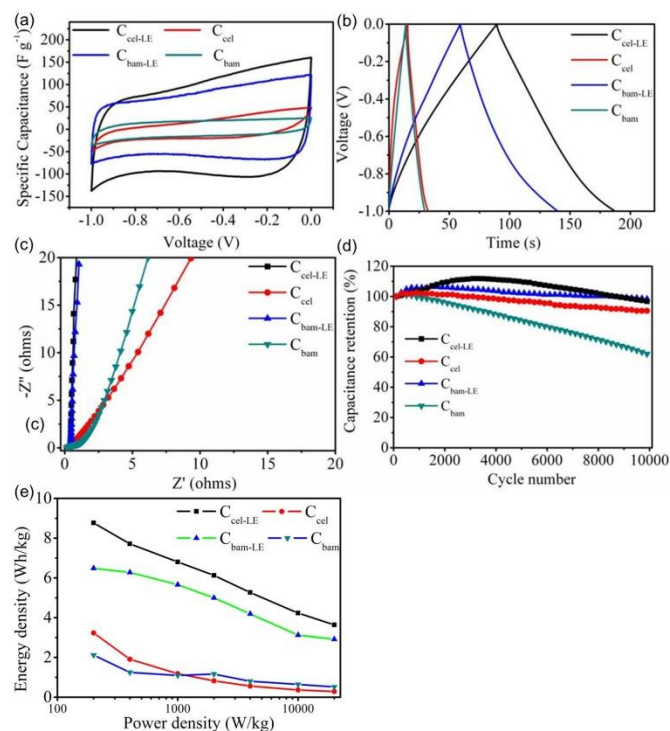


Fig. 5 (a) The CV curves of C_{cel-LE}, C_{cel}, C_{bam-LE}, and C_{bam} tested at 50 mV s⁻¹; and their (b) galvanostatic charge/discharge curves tested at 0.5 A g⁻¹; (c) the corresponding nyquist plots in the frequency range of 100 kHz to 10 mHz in KOH electrolyte; (d) The long cycle life of C_{cel-LE}, C_{cel}, C_{bam-LE}, and C_{bam} over 10 000 cycle numbers at a constant current density of 10 A g⁻¹; (e) Comparisons of energy density and power density between C_{cel-LE}, C_{cel}, C_{bam-LE}, and C_{bam}.

sites and high surface areas, and therefore increase the performance in supercapacitor. More significantly, the voltage drop of $C_{\text{cel-LE}}$ and $C_{\text{bam-LE}}$ at the start of a discharge are 4.86 mV and 3.91 mV, respectively, which are much smaller than C_{cel} 's 14.85 mV and C_{bam} 's 12.69 mV at a current density of 0.5 A g^{-1} . The small IR-drop of $C_{\text{cel-LE}}$ and $C_{\text{bam-LE}}$ suggests a very low equivalent series resistance (ESR), good conductivity and the high mass transfer/diffusion rate of ions into the pores of the samples.^{8,39, 40} Electrochemical impedance spectroscopy (EIS) test (Fig. 5c) was performed over a frequency range from 100 kHz to 10 mHz to further understand the properties of conductivity and ion diffusion in the electrode/electrolyte interface. At the low frequency region, the inclined lines of $C_{\text{cel-LE}}$ and $C_{\text{bam-LE}}$ are close to the theoretical vertical line. These show characteristic features of pure capacitive behavior, indicating the excellent pore accessibility for the electrolyte.⁴¹ Fig. 5d reveals the cycling stability at a constant current density of 10 A g^{-1} . The relative capacitance of $C_{\text{cel-LE}}$ and $C_{\text{bam-LE}}$ would increase at the beginning of the process due to the wetting of the rich porosity.^{42, 43} After 10 000 cycles, the capacitance retention of $C_{\text{cel-LE}}$ and $C_{\text{bam-LE}}$ are 96.5% and 98.4%, respectively, which demonstrate an excellent cycling stability. As for C_{cel} and C_{bam} , only 90.6% and 61.4% of the initial capacitance are retained. Furthermore, the specific energy of the $C_{\text{cel-LE}}$ and $C_{\text{bam-LE}}$ in an aqueous KOH electrolyte are 8.77 and 6.49 Wh/kg, which is more than 2 times higher than that of C_{cel} and C_{bam} , respectively (Fig. 5e). Based on the above experiments, the highly interconnected macropores and mesopores are indeed favorable for a fast diffusion of the transporting ions by minimizing molecular diffusion limitation. The products prepared through "leavening" strategy exhibit high specific capacitance, low ESR and excellent cycling stability.

Conclusion

A novel functional 3D HPCs has been synthesized via a "leavening" strategy. The as-obtained samples demonstrate 3D hierarchically porous nanostructure (containing micro-, meso- and macropores) with high specific surface areas (up to 1893 $m^2 g^{-1}$) and large pore volume (up to 1.37 $cm^3 g^{-1}$). This method is not only easily handled but also demonstrates to be universal for both biomass derivatives and crude biomass. Because of their exceptional nanostructure and surface characteristics, these materials exhibit high capacity (253 F g^{-1}), low ESR and long-term stability. It is believed that this study may provide a new route for the development of novel HPCs-based electrode materials. In addition, it also shows attractive prospects for potential industrial application in energy storage, adsorbent, catalyst, gas storage and so on.

Experimental

Materials, α -cellulose, xylose, glucose, starch, chitin and sucrose were purchased from Aladdin, $KHCO_3$ was purchased from Sinopharm Chemical Reagent Co., Ltd. All chemicals

were analytical grade and used as received. Deionized water was used as the solvent. The bamboo was obtained from the playground of Department of Chemistry, Zhejiang University and dried under the oven. Then, the dried bamboo was ground into powder for further use. Water used throughout all experiments was purified through a Millipore system.

Synthesis of C_{x-LE} , Firstly, biomass (powder) (1.2 g) mixed with Potassium bicarbonate with different mass ratio. Secondly, the mixture was calcined in a Muffle furnace at programmed temperature in N_2 flow (400 mL / min). The temperature program was shown as follow: the temperature rose from ambient temperature to desired temperature remained for another 1 hour (when the calcining temperature is 400 $^{\circ}C$, the thermal treatment time is 3 hours to make sure cellulose polymerize more complete). Heating rate is 15 $^{\circ}C / min$. Later, it began to cool down naturally. Thirdly, after it cooled down to ambient temperature, black solid was gained. Then the black solid was ground into black powder and transferred into a beaker, 60 ml HCl (1:1) was added to the beaker. The mixture was stirred for 6 hours at room temperature. At last, filter the solution and the black solid residue was dried at 70 $^{\circ}C$ in an oven overnight.

Synthesis of C_x , Firstly, carbon precursor (powder) was calcined in a Muffle furnace at the same programmed temperature as C_{x-LE} 's. Then the black solid was ground into black powder.

Characterization

SEM images were obtained on a Hitachi S-4800 and Hitachi SU-70. TEM studies were performed on a Hitachi HT-7700 microscope. The diffraction data were collected at room temperature with 2θ scan range between 10 $^{\circ}$ and 60 $^{\circ}$ using a wide-angle X-ray diffraction (Model D/tex-Ultima TV, 1.6 kV, Rig-aku, Japan) equipped with Cu K α radiation (1.54 \AA). The Raman spectra were collected on a Raman spectrometer (JY, HR 800) using 514-nm laser. The N_2 adsorption-desorption isothermal analysis were determined by micromeritics ASAP 2020 HD88, BET equation was used to calculate the surface areas and pore volume and samples were degassed at 150 $^{\circ}C$ for 6 h until the residual pressure was less than 10 $^{-4}$ Pa. Thermogravimetric Analysis (TGA) was performed using METTLER TOLEDO TGA/DSC 1100SF. Mercury (Hg) porosimetry was performed with AutoPore IV 9510.

Electrochemical characterization

THREE-ELECTRODE TEST SYSTEM: Electrochemical measurements were performed using a computer-controlled workstation (Gamry Reference 600) with a typical three-electrode cell. The working electrodes were prepared by mixing 90 wt% porous carbons as the active materials, 10 wt% polytetrafluoroethylene (PTFE) in 1 mL ethanol to form slurry, and spreading onto a nickel-foam (1 cm \times 1 cm), and dried in infrared fast dryer. The mass load of active material on working electrodes was 4-6 mg cm^{-2} . The foam with sample was compressed before measurement. Electrochemical impedance spectroscopy (EIS) was carried out in 6.0 M KOH with a three-

electrode system by using saturated calomel electrode (SCE) as reference electrode and a platinum electrode as the counter electrode. The EIS was characterized at open circuit potential in the frequency range from 100 kHz to 0.01 Hz with the amplitude 5 mV.

TWO-ELECTRODE TEST SYSTEM: The capacitance performances of all the samples were evaluated in a two-electrode system. A thin film electrode of each sample was prepared by a procedure as described below. Simply, a suspension of porous carbon materials with a concentration of 2.0 mg mL⁻¹ was prepared by ultrasonically dispersing porous carbon materials (10 mg) in a mixture (5 mL) of water, ethanol, and Nafion (Dupont, 5 wt%) with the volume ratio of 4.0: 0.8: 0.2. The suspension (25 μL) was then dropped onto the glassy carbon disk with a diameter of 5 mm and dried thoroughly in infrared oven. Two symmetry electrodes were immersed into a beaker containing 6 mol L⁻¹ KOH solutions, with a distance of 15 mm between the centres. The cell was then connected to a Gamry Reference 600 electrochemical workstation for electrochemical characterization. The capacitance of the supercapacitor cell of the carbon was calculated by the following equation: $C_s = 4I\Delta t/U_m$ (F g⁻¹) where I is the current, Δt the discharge time, U the potential range, and m the total mass of the porous carbon materials on both electrodes.

Acknowledgements

This work was supported by the National Natural Science Foundation of China (21376208 & J1210042), the Zhejiang Provincial Natural Science Foundation for Distinguished Young Scholars of China (LR13B030001), the Specialized Research Fund for the Doctoral Program of Higher Education (J20130060), the Fundamental Research Funds for the Central Universities, the Program for Zhejiang Leading Team of S&T Innovation, the Fundamental Research Funds for the Central Universities and the Partner Group Program of the Zhejiang University and the Max-Planck Society are greatly appreciated.

Notes and references

^a Advanced Materials and Catalysis Group, Center for Chemistry of High-performance and Novel Materials, Department of Chemistry, Zhejiang University, Hangzhou, 310028, P. R. China.

E-mail: chemwy@zju.edu.cn

Electronic Supplementary Information (ESI) available: Elementary, N₂ sorption, Raman, XRD, TEM, and SEM analysis of the prepared C_x-LE. See DOI: 10.1039/b000000x/

- H. Wang, Q. Gao and J. Hu, *J. Am. Chem. Soc.*, 2009, **131**, 7016-7022.
- L. Estevez, R. Dua, N. Bhandari, A. Ramanujapuram, P. Wang and E. P. Giannelis, *Energy Environ. Sci.*, 2013, **6**, 1785-1790.
- G. Srinivas, V. Krungleviciute, Z.-X. Guo and T. Yildirim, *Energy & Environmental Science*, 2014, **7**, 335-342.
- C. M. A. Parlett, K. Wilson and A. F. Lee, *Chem. Soc. Rev.*, 2013, **42**, 3876-3893.
- P. Zhang, J. Yuan, T.-P. Fellinger, M. Antonietti, H. Li and Y. Wang, *Angew. Chem. Int. Ed.*, 2013, **52**, 6028-6032.
- C. Wang, Y. Wang, J. Graser, R. Zhao, F. Gao and M. J. O'Connell, *ACS Nano*, 2013, **7**, 11156-11165.
- L. Wei, M. Sevilla, A. B. Fuertes, R. Mokaya and G. Yushin, *Advanced Energy Materials*, 2011, **1**, 356-361.
- D. C. Guo, J. Mi, G. P. Hao, W. Dong, G. Xiong, W. C. Li and A. H. Lu, in *Energy & Environmental Science*, 2013, vol. 6, pp. 652-659.
- L. Borchardt, M. Oschatz and S. Kaskel, *Materials Horizons*, 2014, **1**, 157-168.
- L. L. Zhang and X. S. Zhao, *Chem. Soc. Rev.*, 2009, **38**, 2520-2531.
- M. Sevilla and R. Mokaya, *Energy & Environmental Science*, 2014, **7**, 1250-1280.
- H. Jiang, P. S. Lee and C. Li, *Energy Environ. Sci.*, 2013, **6**, 41-53.
- D.-W. Wang, F. Li, M. Liu, G. Q. Lu and H.-M. Cheng, *Angew. Chem.*, 2008, **120**, 379-382.
- K. Xia, Q. Gao, J. Jiang and J. Hu, *Carbon*, 2008, **46**, 1718-1726.
- L. Zhang, X. Yang, F. Zhang, G. Long, T. Zhang, K. Leng, Y. Zhang, Y. Huang, Y. Ma, M. Zhang and Y. Chen, *J. Am. Chem. Soc.*, 2013, **135**, 5921-5929.
- M. C. Gutierrez, F. Pico, F. Rubio, J. Manuel Amarilla, F. Javier Palomares, M. L. Ferrer, F. del Monte and J. M. Rojo, *J. Mater. Chem.*, 2009, **19**, 1236-1240.
- F. del Monte, D. Carriazo, M. C. Serrano, M. C. Gutiérrez and M. L. Ferrer, *ChemSusChem*, 2014, **7**, 999-1009.
- S. Dutta, A. Bhaumik and K. C. W. Wu, *Energy & Environmental Science*, 2014, **7**, 3574-3592.
- S. Kubo, R. J. White, K. Tauer and M.-M. Titirici, *Chem. Mater.*, 2013, **25**, 4781-4790.
- J. Lee, S. Han and T. Hyeon, *J. Mater. Chem.*, 2004, **14**, 478-486.
- J. Lee, J. Kim and T. Hyeon, *Adv. Mater.*, 2006, **18**, 2073-2094.
- B. Liu, H. Shioyama, T. Akita and Q. Xu, *J. Am. Chem. Soc.*, 2008, **130**, 5390-5391.
- Z. Sun, Y. Liu, B. Li, J. Wei, M. Wang, Q. Yue, Y. Deng, S. Kaliaguine and D. Zhao, *ACS Nano*, 2013, **7**, 8706-8714.
- M.-M. Titirici, R. J. White, N. Brun, V. L. Budarin, D. S. Su, F. del Monte, J. H. Clark and M. J. MacLachlan, *Chem. Soc. Rev.*, 2015, **44**, 250-290.
- Q. Wang, J. Yan, Y. Wang, T. Wei, M. Zhang, X. Jing and Z. Fan, *Carbon*, 2014, **67**, 119-127.
- J. C. Wang and S. Kaskel, *J. Mater. Chem.*, 2012, **22**, 23710-23725.
- J. Jin, S. Tanaka, Y. Egashira and N. Nishiyama, *Carbon*, 2010, **48**, 1985-1989.
- C. Portet, M. A. Lillo-Rodenas, A. Linares-Solano and Y. Gogotsi, *Phys. Chem. Chem. Phys.*, 2009, **11**, 4943-4945.
- Z. Yue, C. L. Mangun and J. Economy, *Carbon*, 2002, **40**, 1181-1191.
- X. Liu and M. Antonietti, *Carbon*, 2014, **69**, 460-466.
- X. B. Wang, Y. J. Zhang, C. Y. Zhi, X. Wang, D. M. Tang, Y. B. Xu, Q. H. Weng, X. F. Jiang, M. Mitome, D. Golberg and Y. Bando, *Nature Communications*, 2013, **4**.
- F. Kurosaki, H. Koyanaka, M. Tsujimoto and Y. Imamura, *Carbon*, 2008, **46**, 850-857.
- W. Luo, B. Wang, C. G. Heron, M. J. Allen, J. Morre, C. S. Maier, W. F. Stickler and X. Ji, *Nano Lett.*, 2014, **14**, 2225-2229.
- J. i. Hayashi, M. Uchibayashi, T. Horikawa, K. Muroyama and V. G. Gomes, *Carbon*, 2002, **40**, 2747-2752.
- D. Carriazo, M. C. Gutiérrez, F. Picó J. M. Rojo, J. L. G. Fierro, M. L. Ferrer and F. del Monte, *ChemSusChem*, 2012, **5**, 1405-1409.
- M. C. Gutiérrez, D. Carriazo, A. Tamayo, R. Jiménez, F. Picó J. M. Rojo, M. L. Ferrer and F. del Monte, *Chemistry – A European Journal*, 2011, **17**, 10533-10537.
- K. Xie, X. T. Qin, X. Z. Wang, Y. N. Wang, H. S. Tao, Q. Wu, L. J. Yang and Z. Hu, *Adv. Mater.*, 2012, **24**, 347-352.
- X. Yang, J. Zhu, L. Qiu and D. Li, *Adv. Mater.*, 2011, **23**, 2833-2838.
- S. Wang, R. Liu, C. Han, J. Wang, M. Li, J. Yao, H. Li and Y. Wang, *Nanoscale*, 2014.
- Y. Gong, Z. Wei, J. Wang, P. Zhang, H. Li and Y. Wang, *Sci. Rep.*, 2014, **4**.

41. M. D. Stoller and R. S. Ruoff, *Energy & Environmental Science*, 2010, **3**, 1294-1301.
42. C. Cui, W. Qian, Y. Yu, C. Kong, B. Yu, L. Xiang and F. Wei, *J. Am. Chem. Soc.*, 2014, **136**, 2256-2259.
43. Y. Yoon, K. Lee, C. Baik, H. Yoo, M. Min, Y. Park, S. M. Lee and H. Lee, *Adv. Mater.*, 2013, **25**, 4437-4444.

Inspired by Bread Leavening: One-pot Synthesis of Hierarchically Porous Carbon for Supercapacitors

*J. Deng, T. Y. Xiong, F. Xu, M. M. Li, C. L. Han, Y. T. Gong, H. Y. Wang, Prof. Y. Wang**



A simple and universal methodology for carbon materials derived from biomass with hierarchical structure.